Dynamics of Carrier Particles in Two-Component Magnetic Development System of Electrophotography

Hiroyuki Kawamoto, Takashi Hiratsuka, Hideyuki Wakai and Takashi Adachi;
Department of Applied Mechanics and Aerospace Engineering, Waseda University; Tokyo, Japan

Abstract

We have studied dynamics of magnetic brushes in two-component development system of electrophotography by a numerical simulation with an improved Distinct Element Method (DEM) and experimental observation with a high-speed microscope camera. Two-dimensional magnetic field was calculated by superposing measured discrete magnetic flux densities on a development sleeve. It has been calculated and observed that magnetic brushes grow up in the development area inclining in parallel in the direction of the magnetic field and they are crushed by a photoreceptor drum. It has been evaluated that although the total pressure applied to the photoreceptor is almost irrelevant to the diameter of carrier particles, differential force applied by individual chain is dense and small with small particles but rough and large with large particles. This suggests that small carrier particles are preferable to prevent disturbance of developed toner particles on the photoreceptor.

Introduction

Statics and dynamics of magnetic particles in the magnetic field are of great interest in a magnetic brush development system adopted in color and/or high-speed electrophotography machines.[1][2] It is used to develop electrostatic latent images on a photoreceptor drum as shown in Fig. 1. Magnetic carrier beads with electrostatically attached toner particles are introduced into the vicinity of a rotatory sleeve with a stationary magnetic roller inside it. Diameter of carrier particle is several tens micrometer and that of the toner particle is about 10 micrometer. Magnetized carrier beads form chain clusters on the sleeve in the magnetic field as shown in Fig. 1. Tips of chains touch the photoreceptor surface at the development area and toner particles on chains move to electrostatic latent images created by a laser beam on the photoreceptor to form real images. Carrier chains play an important role in this development system in order to realize high-quality printing. Sufficient density and moderate brush force of chains are required to obtain satisfactory image density and to prevent image defects. Therefore, it is necessary to clarify the relationship between kinetic characteristics of formed chains and design parameters, such as the magnetic flux density and physical properties of carrier particles.

In this point of view, the experimental, theoretical, and numerical studies have been conducted on magnetic interaction between magnetic particles. To clarify statics of magnetic particles in the magnetic field, Paranjpe and Elrod formulated the interaction force between magnetic dipoles and determined chain configuration based on a principle of a magnetic potential energy minimization.[3] However, because they assumed a simple row of particles in a straight line, calculated results were elemental and could not

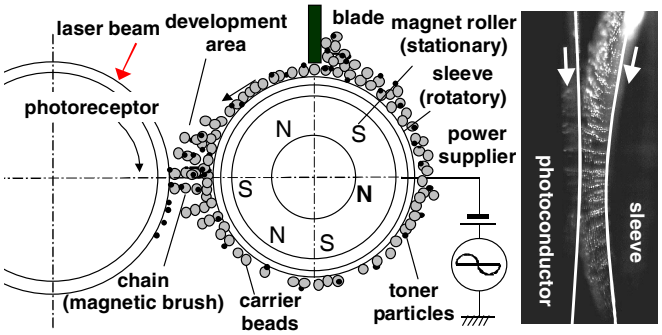

Figure 1. Schematic drawing of two-component magnetic brush development system in electrophotography (left) and photograph of magnetic brushes at development area (right).

simulate the actual complex chains as cited in Fig. 1. We carried out a numerical simulation by the Distinct Element Method (DEM) based on Paranjpe's formulation to clarify the mechanism of the chain formation and to calculate the three-dimensional chain configuration, lateral stiffness of the chain, and resonant frequency of the chain vibration.[4]-[6] Model experiments were also carried out with a solenoid coil for generating the magnetic field and it was demonstrated that the calculation agreed fairly well with the experiment. However, the experiment was elemental and it could not simulate the actual system, because chains were in steady-state and it was not assumed that chains contacted with the photoreceptor. Another issue was that the chain formation was restricted in the magnetic field less than 0.01 T that was limited by the temperature rise of the solenoid coil due to Joule's loss. In this study, dynamic behavior of chains has been observed in an actual developer by a high-speed microscope camera and experimental result has been confirmed by the numerical calculation with an improved Distinct Element Method with a periodic boundary condition to utilize for improvement of the development system.

Numerical Calculation

3D DEM Calculation

Numerical simulation was performed on chain forming process based on the three-dimensional DEM. In the calculation the following momentum equations are solved for each particle j with six degrees of freedom including rotations.[7]

$$m_j \ddot{\boldsymbol{u}}_j = \boldsymbol{F}_j, \quad I_j \ddot{\boldsymbol{\varphi}}_j = \boldsymbol{M}_j, \tag{1}$$

where m_j, $\boldsymbol{u}_j$ (= x_j, y_j, z_j), I_j, $\boldsymbol{\varphi}_j$ (= φ_{xj}, φ_{yj}, φ_{zj}), $\boldsymbol{F}_j$, $\boldsymbol{M}_j$ are mass, displacement vector, moment of inertia, rotation angle, applied force vector, and applied moment to a particle j, respectively. In this

study, mechanical interaction force, magnetic force, air drag, and gravitational force are included in the applied force and the momentum. The mechanical interaction force was estimated based on Voigt model from Hertzian contact theory in the normal direction and Mindlin contact theory in the tangential direction. The magnetic force $\boldsymbol{F}_{mj}$ and rotational moment $\boldsymbol{M}_{mj}$ of the j-th particle with the magnetic moment $\boldsymbol{p}_j$ are given by the following expressions under the assumption that each particle behaves as a magnetic dipole placed at the center of the magnetized particle.

$$\boldsymbol{F}_{mj} = \left(\boldsymbol{p}_j \cdot \nabla\right)\boldsymbol{B}_j, \quad \boldsymbol{M}_{mj} = \boldsymbol{p}_j \times \boldsymbol{B}_j. \tag{2}$$

The magnetic dipole moment $\boldsymbol{p}_j$ and magnetic flux density $\boldsymbol{B}_j$ at the position of the j-th particle are

$$\boldsymbol{B}_j = \boldsymbol{B}_j' + \sum_{\substack{k=1 \\ j \neq k}}^{N} \boldsymbol{B}_{kj}, \tag{3}$$

$$\boldsymbol{p}_j = \frac{4\pi}{\mu_0}\frac{\mu - 1}{\mu + 2}\frac{a_j^3}{8}\boldsymbol{B}_j, \tag{4}$$

where N is the number of particles, μ_0 is the magnetic permeability of free space, μ is the relative permeability of particles, a_j is the diameter of the j-th particle. The first term in the right hand side of Eq. (3) is the applied magnetic field generated by the magnetic roller and the second term is the field at the j-th particle due to dipoles of the other $N-1$ particles. $\boldsymbol{B}_{kj}$ is given by

$$\boldsymbol{B}_{kj} = \frac{\mu_0}{4\pi}\left(\frac{3\boldsymbol{p}_k \cdot \boldsymbol{r}_{kj}}{\left|\boldsymbol{r}_{kj}\right|^5}\boldsymbol{r}_{kj} - \frac{\boldsymbol{p}_k}{\left|\boldsymbol{r}_{kj}\right|^3}\right), \tag{5}$$

where $\boldsymbol{r}_{kj}$ is the position vector from the k-th to the j-th particle. The magnetic force is determined by solving Eqs. (3), (4), and (5) simultaneously and by substituting the calculated results, $\boldsymbol{p}_j$ and $\boldsymbol{B}_j$, to Eq. (2).

A periodical boundary condition is employed to reduce calculation time. In this condition, kinetics of virtually infinite number of particles can be treated with actually small number of particles and thus the calculation time can be reduced. In addition to the calculation time, a realistic calculation can be performed with respect to the chain formation. If the calculation is conducted in a closed box, chains repel magnetically with each other and therefore these are imposed on the wall as shown in Fig. 2 (left pair). This is not actual and eliminated as shown in Fig. 2 (right pair) by adopting the periodical boundary condition.

The calculation is conducted in the domain shown in Fig. 3. The thickness of the domain is 1 mm in the axial direction and it is assumed that this thin domain arrays periodically in the axial longitudinal direction. Firstly, particles are free-fallen on the sleeve and after particles become steady on the sleeve, the sleeve rotates gradually to the rated speed. Total number of 60 μm particles for the numerical calculation is 12,300. The number is coincided to the actual volume density of carrier particles fed to the development

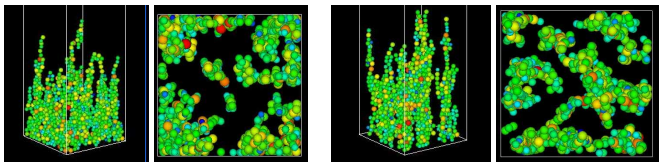

Figure 2. Simulated magnetic brushes with and without periodic boundary condition.

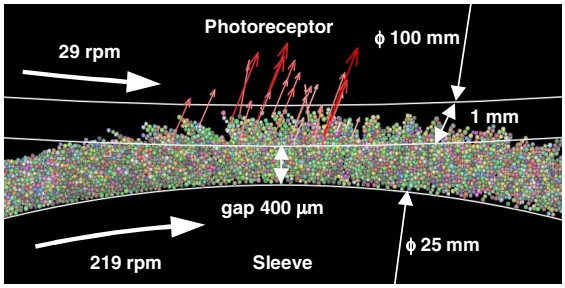

Figure 3. Calculation conditions. Arrows designate pressure of individual chains to the photoreceptor.

area. Not only the chain formation but also the slip speed, pressure, and bulk density are evaluated by the calculation.

Magnetic Field

The magnetic field $\boldsymbol{B}'$ formed by the magnetic roller is estimated from measured discrete data of the magnetic flux density on the sleeve surface based on the assumption that magnetic dipoles distributed on the roller and two-dimensional distribution of the magnetic flux density was calculated by superposing the magnetic flux density created by each dipole. Figure 4 shows a measured distribution of the magnetic flux density on the sleeve and estimated magnetic flux density surrounding the sleeve. It is confirmed that the distribution of the estimated magnetic flux density agrees qualitatively well with an observed profile of brushes in the vicinity of the development gap as shown in Fig. 5.

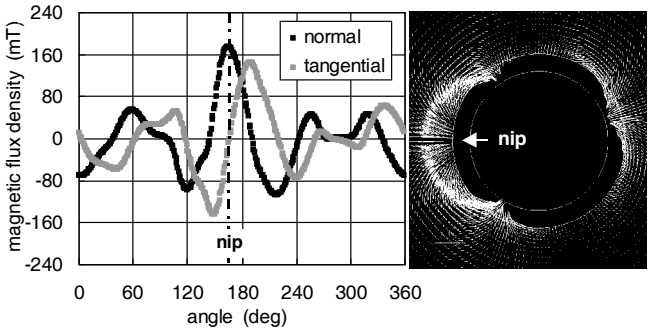

Figure 4. Measured distribution of the magnetic flux density on the sleeve surface (left) and estimated magnetic flux density surrounding the sleeve (right).

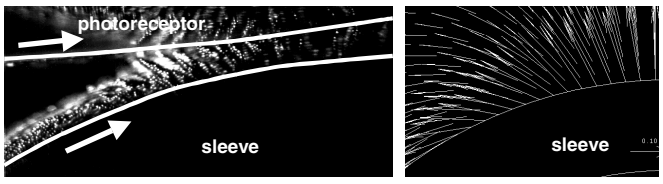

Figure 5. Observed profile of brushes (left) and estimated magnetic flux density (right) in the vicinity of the development gap. Chains are directed to flux lines.

Experimental

Figure 6 shows a schematic drawing of an experimental setup to observe dynamic characteristics of chains at the development area. A mock-up machine was used for the experiment instead of a commercial printer. It enables us to settle an optical apparatus and to change operation parameters such as the gap and the speed of the photoreceptor drum and the development sleeve. A photoconductive film is not coated on the drum but a bare aluminum drum without an insulative coating is used. The development voltage was not applied between the drum and the sleeve to eliminate the effect of the electrostatic force. Dynamic behavior of brushes was observed by a high-speed microscope camera (Photoron, FASTCAM-MAX 120K model 1) at the right end of the development gap. Nominal experimental and numerical conditions are stated in Fig. 2.

Spherical soft-magnetic particles provided by Samsung Yokohama Research Institute were used for the experiment. Toner particles were not mixed with carrier particles. Magnetic carrier particles made of soft ferrite are 42, 50, and 60 μm in average diameter as shown in Fig. 7, 2,200 kg/m^3 in bulk volume density.

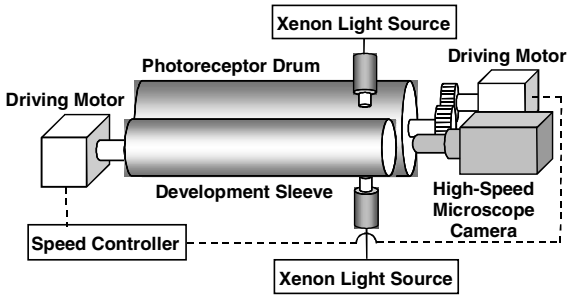

Figure 6. Experimental setup to observe dynamic behavior of chains at development area by high-speed microscope camera.

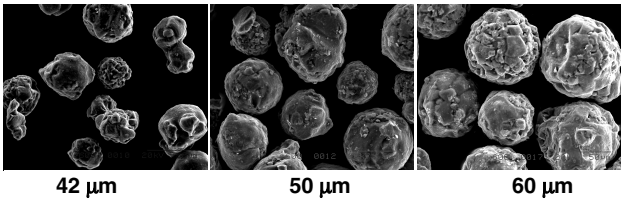

Figure 7. SEM photographs of carrier particles used for experiment.

Results and Discussion

Figure 8 shows calculated and observed behavior of chains at the development area. First of all, it was confirmed that the calculated result agreed fairly well with the observed chain profile. Chains were formed almost parallel to the magnetic flux line designated in calculated figures. At the beginning of the chain formation, chains leaned to the sleeve but these get up gradually when chains approached to the development gap. Then chains contacted the **photoreceptor** drum and depressed by the drum. Chains slipped and swept the drum in this condition. Chains became free again at the back of the development zone and leaned again along the flux line. These characteristics are well recognized both in the DEM calculation and in the experimental observation.

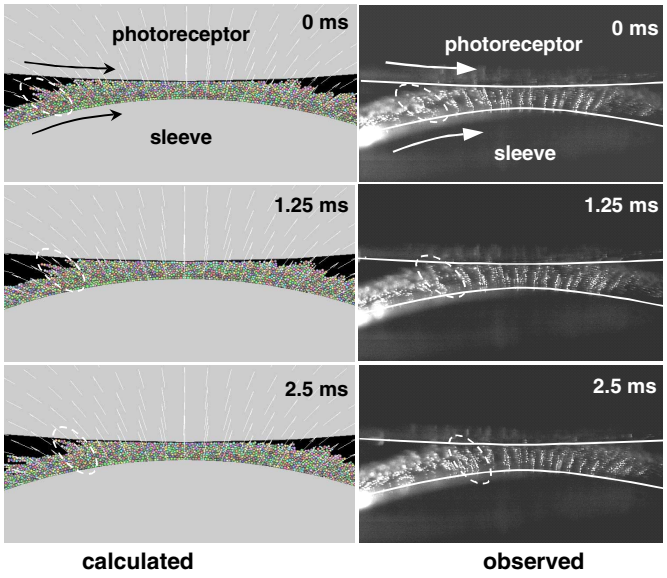

Figure 8. Calculated and observed behavior of chains at development gap.

Figure 9 shows the calculated slip speed of chains to the photoreceptor drum. Time-averaged values are plotted in the figure. The slip speed is slow before chains reach to the center of the development gap, it coincided to the relative speed of the photoreceptor drum and the sleeve, 0.135 m/s, just at the center, and then it becomes higher than the relative speed at the exit of the development area. Finally, chains become free after these pull out of the gap. These features mean that chains are depressed to backward before the center and spring just before chains become free. The springback of chains at the backward of the development area seems to cause a stripe defect of the developed toner images on the photoreceptor if the force applied by chains to the photoreceptor is excessive. In any case, the slip speed is irrelevant to the diameter of the carrier particle.

Figure 10 shows the calculated normal and tangential pressure of chains to the photoreceptor drum. Plotted data in the figure are also time-averaged values. The ratio of the normal and tangential is about 0.35 that coincided to the friction coefficient between the

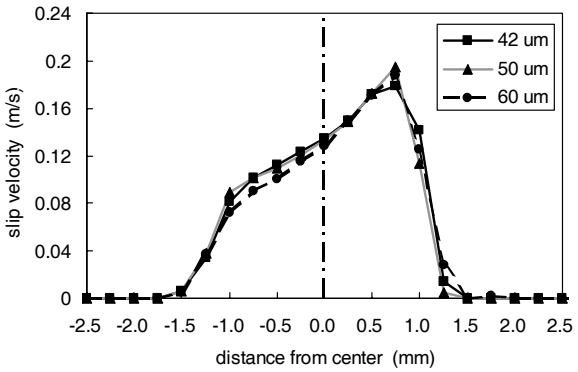

Figure 9. Calculated slip speed of chains to the photoreceptor drum. Relative speed of the photoreceptor drum and the sleeve is 0.135 m/s.

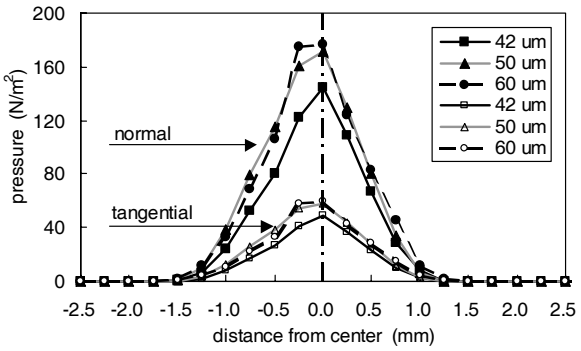

Figure 10. Calculated normal and tangential pressure of chains to the photoreceptor drum.

photoreceptor and carrier particles. The pressure is also almost irrelevant to the diameter of the carrier particle. However, opposite to the distribution of the slip speed, the pressure distribution is almost symmetric with respect to the distance from the center.

The pressure must be moderate to realize sufficient image density and to prevent image defect due to the friction force. That is, if the pressure is too low, sufficient toner particles are not developed, on the other hand, if the pressure is too high, a stripe pattern is developed on the photoreceptor. A parametric calculation was conducted to evaluate the effect of the magnetic field strength, the amount of carrier particles supplied to the gap, and the air gap. It was deduced that the high magnetic field, high bulk density of particles, and small gap cause high pressure. The present calculation method can be utilized to evaluate the effect of these parameters.

Figure 11 shows averaged density of particles that contact with the photoreceptor and Fig. 12 shows differential distribution of the normal pressure applied to the photoreceptor. Distribution of the averaged particle density is almost symmetric with respect to the gap center but it is a little high at the outlet side of the development zone probably due to the friction between chains and photoreceptor. The averaged particle density is inversely proportional to the square of the particle diameter. Although the total pressure applied to the photoreceptor is almost irrelevant to the diameter of carrier particles as shown in Fig. 10, differential force applied by individual chain is dense and small with small particles but, on the other hand, rough

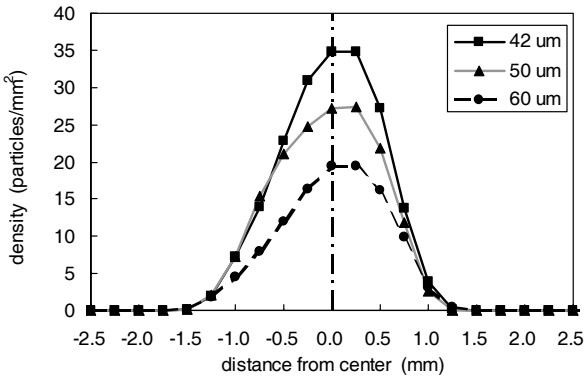

Figure 11. Density of particles that contact with photoreceptor.

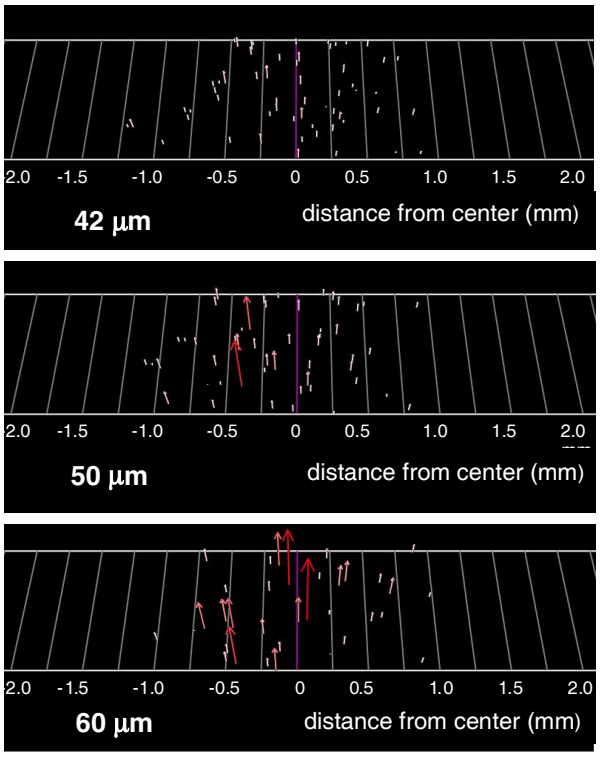

Figure 12. Differential distribution of the normal pressure applied to the photoreceptor. Tangential pressure is 0.35 of the normal pressure.

and large with large particles. This suggests that small carrier particles are preferable to prevent a disturbance of developed images on the photoreceptor.

Concluding Remarks

Dynamics of magnetic brushes in two-component development system of electrophotography has been investigated by an improved Distinct Element Method and the experimental observation with a high-speed microscope camera. The calculated result agreed fairly well to the experimental observation. Although the experimental means are restricted to measure integrated quantities, the calculation method can be utilized to evaluate a detailed dynamic and differential performance. The present experimental and numerical methods are utilized for the improvement of the two-component development system of electrophotography.

This work is supported by Samsung Yokohama Research Institute (SYRI). SYRI provided the mock-up apparatus, carrier particles, and measured data of the magnetic flux density.

References

[1] E. M. Williams, The Physics and Technology of Xerographic Processes, Krieger Publishing, Florida (1993).
[2] L. B. Schein, Electrophotography and Development Physics (Revised Second Edition), Laplacian Press, California (1996).
[3] R. S. Paranjpe and H. G. Elrod, J. Appl. Phys. 60, 418 (1986).
[4] N. Nakayama, H. Kawamoto and M. Yamaguchi, J. Imaging Sci. Technol. 46, 422 (2002).

[5] N. Nakayama, H. Kawamoto, S. Yamada and A. Sasakawa, IS&T's NIP18: International Conference on Digital Printing Technologies, San Diego, 742 (2002).
[6] N. Nakayama, H. Kawamoto and S. Yamada, J. Imaging Sci. Technol. 47, 408 (2003).
[7] P. A. Cundall and O. D. L. Strack, Géotechnique, 29, 47 (1979).

Author Biography

KAWAMOTO, Hiroyuki holds a BS degree in Electrical Engineering from Hiroshima Univ.(1972) and a Dr. degree in Mechanical Engineering from Tokyo Institute of Technology (1983). From 1972 to 1991 he was a Senior Engineer at the Nuclear Division of Hitachi Ltd. In 1991 he moved to Fuji Xerox, and had been engaged in the research of electrophotography as a Research Fellow. In 1999 he left Fuji Xerox and he is now a professor of Waseda Univ. He was selected a Fellow of the IS&T in 1999 and awarded Chester F. Carlson Award in 2007.